JACS
JOURNAL OF THE AMERICAN CHEMICAL SOCIETY

Article

pubs.acs.org/JACS

Designed Formation of $Co_3O_4/NiCo_2O_4$ Double-Shelled Nanocages with Enhanced Pseudocapacitive and Electrocatalytic Properties

Han Hu, Buyuan Guan, Baoyu Xia, and Xiong Wen (David) Lou*

School of Chemical and Biomedical Engineering, Nanyang Technological University, 62 Nanyang Drive, Singapore 637459

Supporting Information

ABSTRACT: Hollow structures with high complexity in shell architecture and composition have attracted tremendous interest because of their great importance for both fundamental studies and practical applications. Herein we report the designed synthesis of novel box-in-box nanocages (NCs) with different shell compositions, namely, $Co_3O_4/NiCo_2O_4$ double-shelled nanocages (DSNCs). Uniform zeolitic imidazolate framework-67/Ni−Co layered double hydroxides yolk-shelled structures are first synthesized and then transformed into $Co_3O_4/NiCo_2O_4$ DSNCs by thermal annealing in air. Importantly, this strategy can be easily extended to prepare other complex DSNCs. When evaluated as electrodes for pseudocapacitors, the $Co_3O_4/NiCo_2O_4$ DSNCs show a high specific capacitance of 972 F g^{-1} at a current density of 5 A g^{-1} and excellent stability with 92.5% capacitance retention after 12 000 cycles, superior to that of Co_3O_4 NCs with simple configuration and Co_3O_4/Co_3O_4 DSNCs. Besides, the $Co_3O_4/NiCo_2O_4$ DSNCs also exhibit much better electrocatalytic activity for the oxygen evolution reaction than Co_3O_4 NCs. The greatly improved electrochemical performance of $Co_3O_4/NiCo_2O_4$ DSNCs demonstrates the importance of rational design and synthesis of hollow structures with higher complexity.

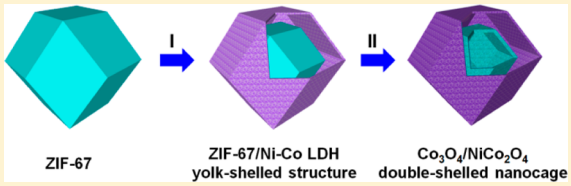

INTRODUCTION

As a unique class of functional materials, hollow micro/nanostructures have attracted tremendous interest for their intriguing structural features and great potential in a myriad of applications including catalysis, drug delivery, and energy storage and conversion systems.[1−9] Over the past decades, a wealth of functional materials has been successfully fabricated into hollow structures with diverse morphologies such as hollow spheres,[4,10] hollow polyhedrons,[6,11,12] and micro/nanotubes.[13,14] However, most of the reported hollow structures are constructed by a single shell of one composition with relatively simple configurations, thus limiting the opportunities for modulating their properties.[2,9] As such, it is highly desirable to design and synthesize hollow structures with high complexity such as multiple shells or multiple compositions.[15,16] For example, Wang et al. reported the synthesis of a series of SnO_2 hollow spheres with single to quintuple shells via a hard-templating process where the multishelled hollow spheres deliver greatly improved performance as photo anodes for dye-sensitized solar cells.[17] We have recently developed a metal−organic frameworks (MOFs) template-engaged method to synthesize multicompositional Fe_2O_3−SnO_2 microboxes which exhibit much better lithium storage performance than the single-compositional microboxes.[16]

Notwithstanding the aforementioned progress to date, the synthesis of complex hollow structures still remains in its infancy as most of the current methods can only realize complex hollow structures either with multishells or with multicompositions.[16−18] Increasing the complexity of hollow structures in a designed manner may bring more possibilities in modulating the properties of functional nanostructures for many applications.[9] However, formation of multishelled hollow structures with different shell compositions has rarely been reported despite the fact that it is conceptually straightforward by a layer-by-layer templating strategy. One reason is due to the difficulties in manipulating different materials with distinct physical/chemical properties simultaneously during the conventional synthesis processes. As such, it is highly desirable yet very challenging to synthesize multishelled hollow structures with different shell compositions.

Herein, we demonstrate a novel approach for the effective synthesis of box-in-box nanocages (NCs) with different shell compositions, namely, $Co_3O_4/NiCo_2O_4$ double-shelled nanocages (DSNCs). This strategy involves the facile synthesis of zeolitic imidazolate framework-67/Ni−Co layered double hydroxides (ZIF-67/Ni−Co LDH) yolk-shelled structures and subsequent thermal annealing in air. Besides, this strategy can be extended to prepare other complex DSNCs. The unique shell architectures and complex compositions endow the $Co_3O_4/NiCo_2O_4$ DSNCs with superior performance when evaluated as electrodes for pseudocapacitors and as electrocatalysts for the oxygen evolution reaction (OER).

EXPERIMENTAL SECTION

Synthesis of ZIF-67 Crystals. All the chemicals were directly used after purchase without further purification. In a typical synthesis, two solutions were first prepared by dissolving 1 mmol of $Co(NO_3)_2{\cdot}6H_2O$ and 4 mmol of 2-methylimidazole in 25 mL of methanol. Then, the solution of 2-methylimidazole was quickly poured into the solution of $Co(NO_3)_2$ and the resultant mixed solution was aged for 24 h at room

Received: March 8, 2015
Published: April 15, 2015

DOI: 10.1021/jacs.5b02465
J. Am. Chem. Soc. 2015, 137, 5590−5595

temperature.[19] The purple precipitate was collected by centrifugation and dried at 70 °C for 6 h. The size of ZIF-67 particles can be easily modulated by varying the amount of 2-methylimidazole, with other conditions unchanged.

Synthesis of $Co_3O_4/NiCo_2O_4$ DSNCs. In total, 40 mg of ZIF-67 templates was first dispersed in 25 mL of ethanol containing 80 mg of $Ni(NO_3)_2{\cdot}6H_2O$. After stirring for 30 min, the ZIF-67/Ni−Co LDH yolk-shelled particles were formed and collected by centrifugation and finally dried at 70 °C for 10 h. Then, the $Co_3O_4/NiCo_2O_4$ DSNCs were obtained by annealing the as-obtained yolk-shelled particles in air at 350 °C for 2 h with a ramp rate of 1 °C min^{-1}.

Synthesis of Co_3O_4 NCs and $NiCo_2O_4$ NCs. The Co_3O_4 NCs were prepared by directly annealing ZIF-67 crystals in air at 350 °C for 2 h with a ramp rate of 1 °C min^{-1}. As for the synthesis of $NiCo_2O_4$ NCs, 40 mg of ZIF-67/Ni−Co LDH yolk-shelled structures was first dispersed in a mixed solvent consisting of 20 mL of ethanol and 5 mL of water and refluxed at 90 °C for 1 h, during which the ZIF-67 cores can be completely removed. Then, the as-obtained Ni−Co LDH NCs were annealed in air at 350 °C for 2 h with a ramp rate of 1 °C min^{-1} to generate the $NiCo_2O_4$ NCs.

Synthesis of Other Complex DSNCs. Other complex DSNCs can be easily realized by reacting ZIF-67 with other metal nitrates. For example, refluxing 40 mg of ZIF-67 in 25 mL of ethanol containing 200 mg of $Mg(NO_3)_2{\cdot}6H_2O$ at 80 °C for 45 min could produce ZIF-67/Mg−Co LDH core-shelled particles. Then, the DSNCs could be synthesized by annealing the as-formed composites at 350 °C for 2 h with a ramp rate of 1 °C min^{-1}. As another example, the ZIF-67 crystals were first stirred in 25 mL of ethanol containing 100 mg of $Co(NO_3)_2{\cdot}6H_2O$ for 1 h. Then the ZIF-67/Co−Co LDH yolk-shelled particles were collected and annealed under the aforementioned conditions, giving rise to the Co_3O_4/Co_3O_4 DSNCs.

Materials Characterization. X-ray diffraction (XRD) patterns were conducted on a Bruker D2 Phaser X-ray diffractometer with Ni filtered Cu Kα radiation (λ = 1.5406 Å) at a voltage of 30 kV and a current of 10 mA. The microstructures were analyzed by field-emission scanning electron microscopy (FESEM; JEOL, JSM-6700F) and transmission electron microscopy (TEM; JEOL, JEM-2010). Energy-dispersive X-ray spectroscopy (EDX) attached to the FESEM was utilized to analyze the composition. Elemental mapping was recorded using EDX spectroscopy attached to TEM (JEOL, JEM-2100F). A Quantachrome Autosorb AS-6B system was used to analyze the specific surface area and porosity of the $Co_3O_4/NiCo_2O_4$ DSNCs and Co_3O_4 NCs.

Evaluation of the Pseudocapacitive Performance. The slurry of the working electrode was prepared by mixing the active material, carbon black (super-P-Li) and polymer binder (polyvinylidene difluoride, PVDF) with a mass ratio of 70:20:10 in *N*-methyl-2-pyrrolidone solvent. Then, the slurry was pasted onto Ni foam followed by drying at 120 °C for 12 h under vacuum. The loading mass of the active material was around 1 mg cm^{-2}. Electrochemical measurements were conducted with a CHI 660C electrochemical workstation via a three-electrode system with a Pt foil serving as the counter electrode and a saturated calomel electrode (SCE) as the reference electrode in an aqueous KOH electrolyte (2.0 M). Both the cyclic voltammetry (CV) curves and chronopotentiometry (CP) curves were measured in a potential range of 0−0.42 V vs SCE. The cycling performance was conducted on a battery tester (NEWARE). The specific capacitance of the electrodes was calculated from the CP curves according to the following equation:

$$C = It/\Delta V \quad (1)$$

where C, I, t, and ΔV are the specific capacitance (F g^{-1}) of the electroactive materials, the discharging current density (A g^{-1}), the discharging time (s), and the discharging potential range (V), respectively.

Evaluation of the Electrocatalytic Activity toward OER. To prepare the electrodes for OER testing, 5 mg of active material was mixed with 0.95 mL of ethanol and 0.05 mL of 5 wt % Nafion solution by sonication for 5 min. Then, the suspension was carefully drop dried onto a piece of 1 cm × 1 cm Ni foam to achieve the active material loading of 1 mg. The catalytic activity was tested in a standard three-electrode system with a CHI 660D electrochemical workstation in 1.0 M KOH solution. The counter electrode and reference electrode were a Pt foil and a SCE, respectively. All the measured potentials were referred to RHE with the following equation:

$$E(\mathrm{RHE}) = E(\mathrm{SCE}) + 1.068 \quad (2)$$

Linear sweep voltammetry was carried out at a scan rate of 5 mV s^{-1} for the polarization curves. The I−t curve was measured under a fixed overpotential of 0.34 V. All polarization curves were iR corrected. The electrochemical double-layer capacitance was determined from the CV curves measured in a potential range without redox processes according to the following equation:

$$C_{dl} = I_c/\nu \quad (3)$$

where C_{dl}, I_c, and ν are the double-layer capacitance (F cm^{-2}) of the electroactive materials, charging current (mA cm^{-2}), and scan rate (mV s^{-1}).

RESULTS AND DISCUSSION

The synthesis process of $Co_3O_4/NiCo_2O_4$ DSNCs is schematically illustrated in Figure 1. Two methanol solutions of $Co(NO_3)_2$ and 2-methylimidazoleare mixed rapidly and aged for 24 h at room temperature to generate uniform ZIF-67 ($Co(MeIM)_2$, MeIM = 2-methylimidazole) particles which serve as templates.[19,20] In the first step, these ZIF-67 particles are dispersed in ethanol solution of $Ni(NO_3)_2$ and continuously stirred for 30 min to produce ZIF-67/Ni−Co LDH yolk-shelled structures.[19] During the process, protons generated from the hydrolysis of Ni^{2+} ions can gradually etch ZIF-67 templates and the released Co^{2+} ions may be partially oxidized by dissolved O_2 and NO_3^- ions in the solution. Then the Co^{2+}/Co^{3+} ions will coprecipitate with Ni^{2+} ions to form Ni−Co LDH shells.[19,21] Afterward, thermal calcination is applied during which the ZIF-67 cores and Ni−Co LDH shells can be converted into Co_3O_4 and $NiCo_2O_4$ NCs, respectively. Because of the as-formed gap between ZIF-67 and Ni−Co LDH, possible strain between the cores and the shells generated during the calcination process that may result in the collapse of the shells can be effectively alleviated. Thus, both the inner Co_3O_4 shell and the outer $NiCo_2O_4$ shell can remain intact, giving rise to the $Co_3O_4/NiCo_2O_4$ DSNCs. Therefore, the difficulties in forming multi-shelled hollow structures with different shell materials by conventional layer-by-layer templating methods have been effectively circumvented.

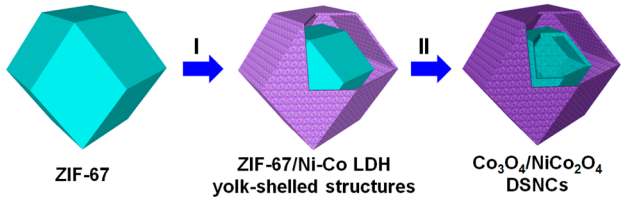

Figure 1. Schematic illustration of the formation process of $Co_3O_4/NiCo_2O_4$ DSNCs. Step I: transformation of ZIF-67 into ZIF-67/Ni−Co LDH yolk-shelled structures by a facile etching and deposition process. Step II: formation of $Co_3O_4/NiCo_2O_4$ DSNCs by annealing the yolk-shelled structures in air.

The structures formed at different steps are characterized by powder X-ray diffraction (XRD), energy-dispersive X-ray spectroscopy (EDX), field-emission scanning electron microscopy (FESEM), and transmission electron microscopy (TEM). The XRD pattern of the ZIF-67 crystals matches well with

DOI: 10.1021/jacs.5b02465
J. Am. Chem. Soc. 2015, 137, 5590−5595

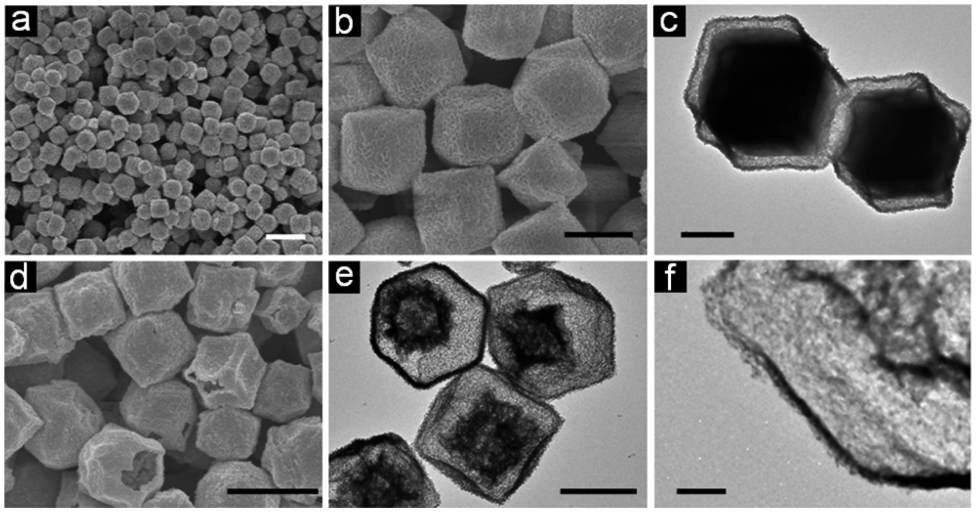

Figure 2. FESEM (a, b, d) and TEM (c, e, f) characterizations of samples. (a, b, c) ZIF-67/Ni−Co LDH yolk-shelled structures formed by reacting ZIF-67 with $Ni(NO_3)_2$ for 30 min in ethanol; (d, e, f) $Co_3O_4/NiCo_2O_4$ DSNCs formed by thermal annealing the ZIF-67/Ni−Co LDH yolk-shelled structures in air at 350 °C for 2 h with a ramp rate of 1 °C min^{-1}. Scale bars, 2 μm in part a; 500 nm in parts b and e; 300 nm in part c; 1 μm in part d; 100 nm in part f.

previous reports,[19,20] and the EDX result confirms the stoichiometry[22−24] of the as-prepared crystals (Figure S1a,b, Supporting Information). FESEM and TEM images (Figure S1c,d, Supporting Information) reveal that the ZIF-67 particles show a polyhedral shape with a smooth surface and an average size of approximately 800 nm. After reaction with $Ni(NO_3)_2$ in ethanol solution for 30 min, the particles still retain a polyhedral shape but exhibit a rougher surface constructed by small nanosheets, as shown in Figure 2a,b. XRD pattern demonstrates these polyhedrons are still mainly ZIF-67 with diminished peak intensity, further confirmed by the EDX analysis (Figure S2a,b, Supporting Information). FESEM image of a particle with a broken outer shell (Figure S2c, Supporting Information) reveals that the inner core preserves the smooth surface. The distinctions between the shell and the core are further revealed by TEM observations (Figure 2c and Figure S2d, Supporting Information) where the shell is composed of interconnected small nanosheets while the core appears similar to ZIF-67. Meanwhile, a well-developed gap can be discerned from these TEM images which may play a crucial role on the formation of DSNCs. To determine the structure and composition of the outer shell, the ZIF-67 core with poor water stability is removed by refluxing in a mixed solvent of ethanol and water at elevated temperature.[22,24] After that, the diffraction peaks of ZIF-67 are totally absent in the XRD pattern (Figure S3a, Supporting Information) and the (003), (006), (009), and (110) peaks are unambiguously ascribed to a typical LDH structure.[19,21] This result strongly supports the successful formation of ZIF-67/Ni−Co LDH yolk-shelled structures by reacting ZIF-67 with $Ni(NO_3)_2$. EDX spectrum of the Ni−Co LDH shows a Ni/Co molar ratio of around 0.53 (Figure S3b, Supporting Information). FESEM and TEM images (Figure S3c,d, Supporting Information) show the fully hollowed Ni−Co LDH NCs indicating the complete removal of the ZIF-67 cores. The thermal annealing of ZIF-67 crystals and Ni−Co LDH NCs can result in the formation of spinel type Co_3O_4 (Figure S4a,b, Supporting Information) and $NiCo_2O_4$ (Figure S5a,b, Supporting Information), respectively.[25,26] Both of the annealed products show cage-like structures (Figures S4c,d, and S5c,d, Supporting Information), which gives the possibility of formation of box-in-box DSNCs with different shell compositions by annealing ZIF-67/Ni−Co LDH yolk-shelled structures. XRD pattern of the annealed product of ZIF-67/Ni−Co LDH yolk-shelled structures confirms the formation of the spinel type oxides containing Ni and Co (Figure S6a,b, Supporting Information). From a panoramic FESEM image (Figure S6c, Supporting Information), the annealed product inherits the polyhedral shape from the ZIF-67/Ni−Co LDH yolk-shelled structures. Furthermore, the inner shell can be well identified from some particles with broken outer shells (Figure 2d). From TEM observations (Figure 2e and Figure S6d, Supporting Information), the NCs derived from the Ni−Co LDH do not shrink significantly whereas the inner NCs derived from ZIF-67 show significant shrinkage with decreased size compared with the original ZIF-67 cores. The thickness of the shells has been determined by TEM observation under higher magnification. As shown in Figure 2f, the thickness of the outer $NiCo_2O_4$ shell is about 20 nm while the inner Co_3O_4 shell shows similar thickness but with a very uneven surface.

The spatial distribution of different elements in the $Co_3O_4/NiCo_2O_4$ DSNCs is investigated by elemental mapping analysis on a representative $Co_3O_4/NiCo_2O_4$ DSNC under TEM observation. The elemental mapping results indicate that Co (Figure 3a,b) and O (Figure 3a,d) are distributed homogeneously in both the outer shell and the inner shell with some apparent enhancement in the central region. On the contrary, the signal intensity of Ni (Figure 3a,c) is very uniform throughout the region without any enhancement in the central area where the inner Co_3O_4 NC locates, indicating the inner shell is free of Ni. Thus, these EDX results further verify that the inner shell mainly consists of Co_3O_4, and the outer shell is composed of $NiCo_2O_4$, confirming the successful formation of DSNCs with different shell compositions.

To get further insight into the formation process of high-quality $Co_3O_4/NiCo_2O_4$ DSNCs, ZIF-67/Ni−Co LDH particles generated at different durations have been annealed and characterized by FESEM and TEM observations. ZIF-67/Ni−Co LDH core-shelled structures are formed with a short duration of only 15 min where the outer shell is tightly adhered on the surface of the ZIF-67 crystal (Figure S7a,c, Supporting Information). The annealed product observed by FESEM and

DOI: 10.1021/jacs.5b02465
J. Am. Chem. Soc. 2015, 137, 5590−5595

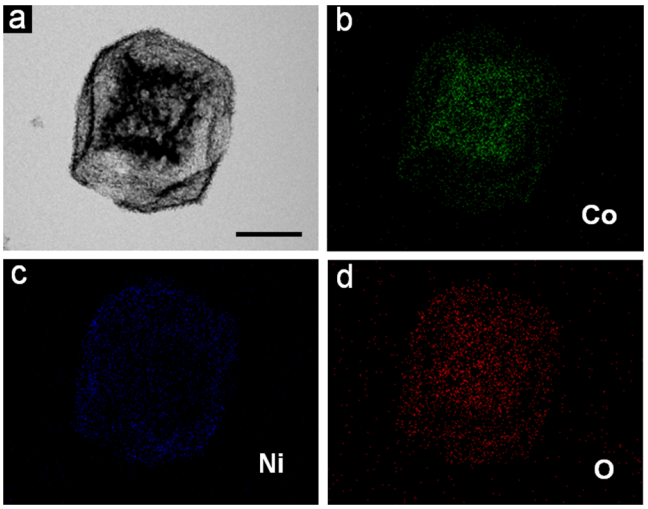

Figure 3. Elemental mapping of the $Co_3O_4/NiCo_2O_4$ DSNCs. (a) TEM image of an individual $Co_3O_4/NiCo_2O_4$ DSNC and elemental mapping of Co (b), Ni (c), and O (d). Scale bar in part a is 300 nm.

TEM (Figure S7b,d, Supporting Information) still shows a cage-like morphology whereas well-defined double-shells cannot be developed because of the different volume shrinkage of Ni−Co LDH and ZIF-67 during the thermal annealing process (Figures S4c,d, S5c,d, and S6c,d, Supporting Information). As such, cracked inner shells are observed (Figure S7d, Supporting Information). If the reaction duration is extended to 2 h, the as-obtained particles are heavily aggregated (Figure S8a,c, Supporting Information). As a result, it is difficult to obtain uniform discrete DSNCs in the annealed product (Figure S8b,d, Supporting Information).

The strategy developed here is highly versatile and can be conducted on ZIF-67 polyhedrons with different sizes, thus enabling size-controllable synthesis of $Co_3O_4/NiCo_2O_4$ DSNCs. As a demonstration, DSNCs with sizes around 500 nm and 1.5 μm have been successfully produced (Figure S9, Supporting Information). On the other hand, a series of Co-containing LDH structures can be easily synthesized by reacting ZIF-67 with different metal nitrates.[19] Thus, several kinds of DSNCs with inner Co_3O_4 NCs and outer NCs of other metal oxides can be formed via the present strategy. For example, by refluxing ZIF-67 particles in ethanol solution of $Mg(NO_3)_2$ at elevated temperature, ZIF-67/Mg−Co LDH core-shelled particles can be formed. The Mg−Co LDH nanosheets in the outer shells (Figure S10a,c, Supporting Information) are much larger than Ni−Co LDH nanosheets. After annealing, the DSNCs (Figure S10b,d, Supporting Information) can be obtained and the elemental distribution in these DSNCs is determined by EDX mapping under TEM observation (Figure S11, Supporting Information). If the ZIF-67 crystals are stirred in ethanol solution of $Co(NO_3)_2$, ZIF-67/Co−Co LDH yolk-shelled particles (Figure S12a,c, Supporting Information) can be formed which will be converted into Co_3O_4/Co_3O_4 DSNCs (Figures S12b,d, and S13, Supporting Information) after thermal annealing.

The $Co_3O_4/NiCo_2O_4$ DSNCs show a specific surface area of 46 $m^2\ g^{-1}$ with suitable pore size distribution (Figure S14a, Supporting Information) that may bring interesting pseudocapacitive properties.[27] As such, the pseudocapacitive performance of $Co_3O_4/NiCo_2O_4$ DSNCs is investigated by using a three-electrode system with a Pt foil as the counter electrode and a SCE as the reference electrode in 2.0 M KOH aqueous electrolyte. One representative cyclic voltammetry (CV) curve at a constant scan rate of 2 mV s^{-1} in a potential window of 0−0.42 V is given in Figure 4a, together with another CV curve of Co_3O_4 NCs with a smaller specific surface area of 15.2 $m^2\ g^{-1}$ (Figure S14b, Supporting Information) under identical conditions for comparison. As shown, the distinct redox peaks are observed during the anodic and cathodic sweeps which deliver the faradic pseudocapacitance based on surface reactions.[28] Because of the similar redox potentials of Ni^{2+}/Ni^{3+} and Co^{3+}/Co^{4+}, the

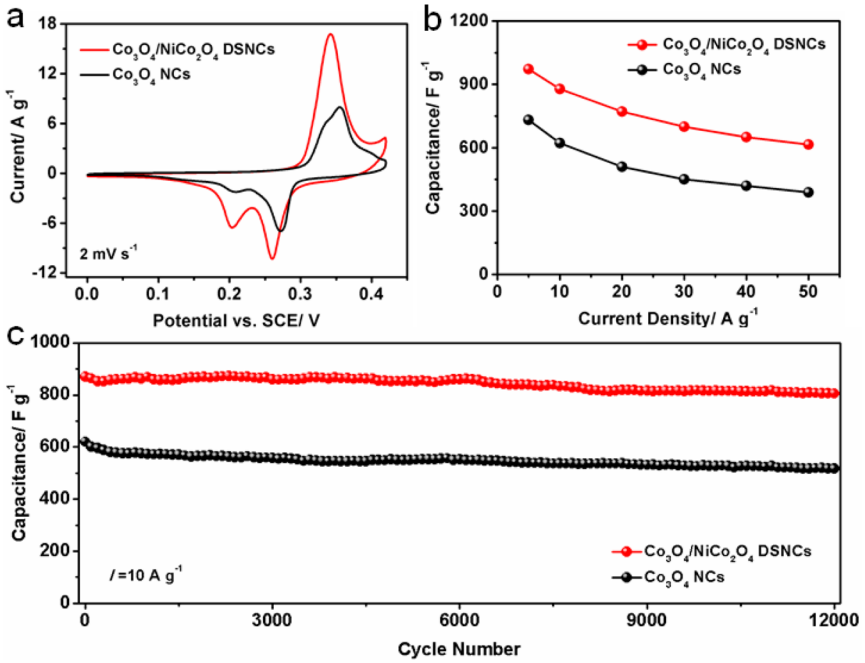

Figure 4. Electrochemical characterizations of the $Co_3O_4/NiCo_2O_4$ DSNCs and Co_3O_4 NCs. (a) Cyclic voltammetry (CV) curves at a scan rate of 2 mV s^{-1}; (b) specific capacitance as a function of current density; and (c) cycling performance at a current density of 10 A g^{-1}.

DOI: 10.1021/jacs.5b02465
J. Am. Chem. Soc. 2015, 137, 5590−5595

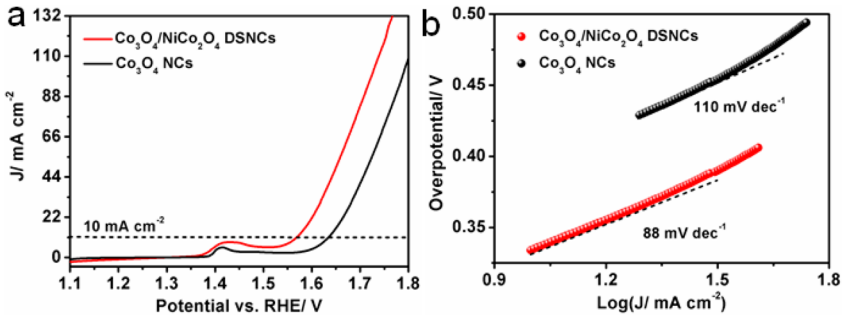

Figure 5. Electrocatalytic activity of the $Co_3O_4/NiCo_2O_4$ DSNCs and Co_3O_4 NCs for OER. (a) Polarization curves and (b) Tafel plots in 1.0 M KOH solution (5 mV s^{-1}).

positions of the redox peaks for both electrodes are almost identical.[29] With the increasing scan rate from 2 to 50 mV s^{-1}, the shape of the CV curves shows little evolution except for the slight shift of peak positions. Interestingly, the CV curves of $Co_3O_4/NiCo_2O_4$ DSNCs enclose much larger areas than those of Co_3O_4 NCs at all tested scan rates (Figure S15a,b, Supporting Information). Thus, a larger amount of charges can be stored in the $Co_3O_4/NiCo_2O_4$ DSNCs.

The chronopotentiometry (CP) curves of the $Co_3O_4/NiCo_2O_4$ DSNCs in the voltage range of 0 to 0.42 V at different current densities are presented in Figure S15c, Supporting Information. The voltage plateaus observed in the charge/discharge curves match well with the CV measurement. Also, the durations for charging and discharging are almost identical at all current rates, revealing the excellent reversibility of these redox reactions.[12] The specific capacitance as a function of current density calculated from CP curves (Figure S15c,d, Supporting Information) is plotted in Figure 4b. The $Co_3O_4/NiCo_2O_4$ DSNCs exhibit a high capacitance of 972 F g^{-1} at a current density of 5 A g^{-1} and an impressive capacitance as high as 615 F g^{-1} can be delivered even at a current density of 50 A g^{-1}. This means that 63.2% of the capacitance can be retained with the 10-fold increase in current density from 5 to 50 A g^{-1}, indicating superior rate capability. Compared with $Co_3O_4/NiCo_2O_4$ DSNCs, the Co_3O_4 NCs deliver inferior performance in terms of much lower specific capacitance and poor rate capability. Furthermore, the electrochemical stability over cycling is evaluated at a current density of 10 A g^{-1} by repeated charging and discharging for 12 000 cycles. As shown in Figure 4c, the specific capacitance of 870 F g^{-1} for the first cycle gradually decreases to a value of 805 F g^{-1} after 12 000 cycles with capacitance retention of 92.5%. The superior cycling stability is likely related to the excellent structural stability of the $Co_3O_4/NiCo_2O_4$ DSNCs. From the post-mortem study (Figure S16, Supporting Information), the structure of DSNCs is well maintained without significant deterioration after charging/discharging for 12 000 cycles. On the other hand, the Co_3O_4 NCs show a capacitance loss of 16.6% (Figure 4c) over 12 000 cycles. The pseudocapacitive performance of $Co_3O_4/NiCo_2O_4$ DSNCs has been further compared with that of Co_3O_4/Co_3O_4 DSNCs (Figure S17, Supporting Information). The capacitance retention for the Co_3O_4/Co_3O_4 DSNCs is only 48% when increasing the current density from 5 to 50 A g^{-1}. In addition, the Co_3O_4/Co_3O_4 DSNCs also deliver inferior cycling stability as revealed by a larger capacitance loss of 24.2% after charging/discharging for 12 000 cycles.

Many spinel cobaltite oxides show promising electrocatalytic properties for a myriad of electrochemical reactions such as OER.[30−32] We therefore also investigate the electrocatalytic activity of these $Co_3O_4/NiCo_2O_4$ DSNCs and Co_3O_4 NCs for OER. Figure 5a shows the polarization curves of $Co_3O_4/NiCo_2O_4$ DSNCs and Co_3O_4 NCs. Evidently, a significant oxidation wave with an onset potential of 1.53 V relative to the reversible hydrogen electrode (RHE) associated with electrocatalytic water oxidation[33,34] can be observed for $Co_3O_4/NiCo_2O_4$ DSNCs while the onset potential for Co_3O_4 NCs appears at a very positive position of 1.57 V. The influence from the conductive substrate can be eliminated due to its extremely poor activity (Figure S18, Supporting Information).[35,36] The potential required for a current density of 10 mA cm^{-2}, which is a metric associated with solar fuel synthesis,[37] for different electrodes has been further compared. As shown, the $Co_3O_4/NiCo_2O_4$ DSNCs deliver a current density of 10 mA cm^{-2} at a potential of 1.57 V, whereas a potential as high as 1.64 V is required for Co_3O_4 NCs to achieve the same current density. Moreover, these $Co_3O_4/NiCo_2O_4$ DSNCs outperform many other integrated electrodes such as $Ni_xCo_{3-x}O_4$ nanowire arrays on Ti foil, Ni-substituted Co_3O_4 nanowire arrays on Ni foam, and so on.[29,38] The OER kinetics of these two electrodes is estimated by their corresponding Tafel plots. As shown in Figure 5b, the Tafel slope of the $Co_3O_4/NiCo_2O_4$ DSNCs is 88 mV dec^{-1} compared to 110 mV dec^{-1} for Co_3O_4 NCs. Further, the electrochemical double-layer capacitance (C_{dl}), which is believed to be positively proportional to the electrochemical active surface area (ECSA), is determined by measuring the CV curves in the potential range of 1.25−1.30 V without redox processes.[29,39] As can be seen, the C_{dl} of $Co_3O_4/NiCo_2O_4$ DSNCs is much larger than that of Co_3O_4 NCs (Figure S19, Supporting Information). This might provide some explanation for the much enhanced electrocatalytic performance observed from the $Co_3O_4/NiCo_2O_4$ DSNCs. Besides the catalytic activity, stability represents another crucial factor in the development of reliable electrocatalysts for water splitting.[31,33,34,40] The current of the $Co_3O_4/NiCo_2O_4$ DSNCs at a fixed overpotential of 0.34 V has been monitored for 10 h (Figure S20, Supporting Information), during which the current remains almost constant. A post-mortem study has revealed that the structure of these $Co_3O_4/NiCo_2O_4$ DSNCs is largely retained (Figure S21, Supporting Information).

The electrochemical properties in terms of pseudocapacitive performance and OER activity of the $Co_3O_4/NiCo_2O_4$ DSNCs are superior to those of Co_3O_4 NCs with a simple configuration. The greatly improved performance may largely be attributed to the composition and complex structure of the $Co_3O_4/NiCo_2O_4$ DSNCs. Specifically, the incorporation of Ni^{2+} cations into the spinel structures could result in the increased conductivity and the creation of new active sites.[29,41] Also, the complex porous structure with much higher specific surface area should be also

DOI: 10.1021/jacs.5b02465
J. Am. Chem. Soc. 2015, 137, 5590−5595

beneficial for electrochemical applications.[33] This may well explain the higher specific pseudocapacitance and electrocatalytic activity of the $Co_3O_4/NiCo_2O_4$ DSNCs. Moreover, the unique double-shelled structures may lead to the confinement of the electrolyte between the shells and higher instantaneous concentration can be expected, leading to a higher driving force for the electrochemical reactions.[42] Furthermore, the double-shelled structure is believed to be more structurally robust which is important for the enhanced electrochemical stability for both pseudocapacitors and OER.

CONCLUSIONS

In summary, a novel two-step strategy has been developed to synthesize $Co_3O_4/NiCo_2O_4$ double-shelled nanocages (DSNCs). The synthesis process involves the formation of ZIF-67/Ni−Co LDH yolk-shelled structures with a polyhedral shape and subsequent thermal annealing in air. This strategy can be easily extended to synthesize other complex DSNCs. When evaluated as electrodes for pseudocapacitors and electrocatalysts for oxygen evolution reaction (OER), the $Co_3O_4/NiCo_2O_4$ DSNCs outperform single-shelled Co_3O_4 nanocages and many other related materials. This work may inspire rational creation of complex hollow structures with enhanced properties for a variety of applications.

ASSOCIATED CONTENT

Supporting Information

FESEM images, TEM images, EDX spectra, and XRD patterns of materials at different stages and detailed electrochemical characterization of $Co_3O_4/NiCo_2O_4$ DSNCs, Co_3O_4 NCs, and Co_3O_4/Co_3O_4 DSNCs. This material is available free of charge via the Internet at http://pubs.acs.org.

AUTHOR INFORMATION

Corresponding Author

*E-mail: xwlou@ntu.edu.sg; davidlou88@gmail.com.

Notes

The authors declare no competing financial interest.

ACKNOWLEDGMENTS

We are grateful to the Ministry of Education (Singapore) for financial support through the AcRF Tier-1 funding (Grant RG12/13, M4011154).

REFERENCES

(1) Oh, M. H.; Yu, T.; Yu, S. H.; Lim, B.; Ko, K. T.; Willinger, M. G.; Seo, D. H.; Kim, B. H.; Cho, M. G.; Park, J. H.; Kang, K.; Sung, Y. E.; Pinna, N.; Hyeon, T. *Science* **2013**, *340*, 964.
(2) Lou, X. W.; Archer, L. A.; Yang, Z. C. *Adv. Mater.* **2008**, *20*, 3987.
(3) Liu, J.; Yang, H. Q.; Kleitz, F.; Chen, Z. G.; Yang, T. Y.; Strounina, E.; Lu, G. Q.; Qiao, S. Z. *Adv. Funct. Mater.* **2012**, *22*, 591.
(4) Hu, J.; Chen, M.; Fang, X. S.; Wu, L. W. *Chem. Soc. Rev.* **2011**, *40*, 5472.
(5) Dong, Z. H.; Lai, X. Y.; Halpert, J. E.; Yang, N. L.; Yi, L. X.; Zhai, J.; Wang, D.; Tang, Z. Y.; Jiang, L. *Adv. Mater.* **2012**, *24*, 1046.
(6) Nai, J. W.; Tian, Y.; Guan, X.; Guo, L. *J. Am. Chem. Soc.* **2013**, *135*, 16082.
(7) Liu, J.; Qiao, S. Z.; Chen, J. S.; Lou, X. W.; Xing, X. R.; Lu, G. Q. *Chem. Commun.* **2011**, *47*, 12578.
(8) Joo, J. B.; Dahl, M.; Li, N.; Zaera, F.; Yin, Y. D. *Energy Environ. Sci.* **2013**, *6*, 2082.
(9) Lai, X. Y.; Halpert, J. E.; Wang, D. *Energy Environ. Sci.* **2012**, *5*, 5604.
(10) Yin, Y. D.; Rioux, R. M.; Erdonmez, C. K.; Hughes, S.; Somorjai, G. A.; Alivisatos, A. P. *Science* **2004**, *304*, 711.
(11) Wang, Z. Y.; Lou, X. W. *Adv. Mater.* **2012**, *24*, 4124.
(12) Yu, L.; Zhang, L.; Wu, H. B.; Lou, X. W. *Angew. Chem., Int. Ed.* **2014**, *53*, 3711.
(13) Qu, X.; Kobayashi, N.; Komatsu, T. *ACS Nano* **2010**, *4*, 1732.
(14) Dickey, M. D.; Weiss, E. A.; Smythe, E. J.; Chiechi, R. C.; Capasso, F.; Whitesides, G. M. *ACS Nano* **2008**, *2*, 800.
(15) Zhang, G. Q.; Xia, B. Y.; Xiao, C.; Yu, L.; Wang, X.; Xie, Y.; Lou, X. W. *Angew. Chem., Int. Ed.* **2013**, *52*, 8643.
(16) Zhang, L.; Wu, H. B.; Lou, X. W. *J. Am. Chem. Soc.* **2013**, *135*, 10664.
(17) Dong, Z. H.; Lai, X. Y.; Halpert, J. E.; Yang, N. L.; Yi, L. X.; Zhai, J.; Wang, D.; Tang, Z. Y.; Jiang, L. *Adv. Mater.* **2012**, *24*, 1046.
(18) Yu, X. Y.; Yu, L.; Shen, L. F.; Song, X. H.; Chen, H. Y.; Lou, X. W. *Adv. Funct. Mater.* **2014**, *24*, 7440.
(19) Jiang, Z.; Li, Z. P.; Qin, Z. H.; Sun, H. Y.; Jiao, X. L.; Chen, D. R. *Nanoscale* **2013**, *5*, 11770.
(20) Wu, R. B.; Qian, X. K.; Rui, X. H.; Liu, H.; Yadian, B. L.; Zhou, K.; Wei, J.; Yan, Q. Y.; Feng, X. Q.; Long, Y.; Wang, L. Y.; Huang, Y. Z. *Small* **2014**, *10*, 1932.
(21) Fan, G. L.; Li, F.; Evans, D. G.; Duan, X. *Chem. Soc. Rev.* **2014**, *43*, 7040.
(22) Chen, B. L.; Yang, Z. X.; Zhu, Y. Q.; Xia, Y. D. *J. Mater. Chem. A* **2014**, *2*, 16811.
(23) Xia, W.; Zhu, J. H.; Guo, W. H.; An, L.; Xia, D. G.; Zou, R. Q. *J. Mater. Chem. A* **2014**, *2*, 11606.
(24) Sindoro, M.; Yanai, N.; Jee, A. Y.; Granick, S. *Acc. Chem. Res.* **2014**, *47*, 459.
(25) Lu, Y. Y.; Zhan, W. W.; He, Y.; Wang, Y. T.; Kong, X. J.; Kuang, Q.; Xie, Z. X.; Zheng, L. S. *ACS. Appl. Mater. Interfaces* **2014**, *6*, 4186.
(26) Hu, L. F.; Wu, L. M.; Liao, M. Y.; Hu, X. H.; Fang, X. S. *Adv. Funct. Mater.* **2012**, *22*, 998.
(27) Wei, T. Y.; Chen, C. H.; Chien, H. C.; Lu, S. Y.; Hu, C. C. *Adv. Mater.* **2010**, *22*, 347.
(28) Yuan, C. Z.; Li, J. Y.; Hou, L. R.; Zhang, X. G.; Shen, L. F.; Lou, X. W. *Adv. Funct. Mater.* **2012**, *22*, 4592.
(29) Lu, B. A.; Cao, D. X.; Wang, P.; Wang, G. L.; Gao, Y. Y. *Int. J. Hydrogen Energy* **2011**, *36*, 72.
(30) Hamdani, M.; Singh, R. N.; Chartier, P. *Int. J. Electrochem. Sci.* **2010**, *5*, 556.
(31) Liang, Y. Y.; Li, Y. G.; Wang, H. L.; Zhou, J. G.; Wang, J.; Regier, T.; Dai, H. J. *Nat. Mater.* **2011**, *10*, 780.
(32) Maiyalagan, T.; Jarvis, K. A.; Therese, S.; Ferreira, P. J.; Manthiram, A. *Nat. Commun.* **2014**, *5*, 3949.
(33) Ma, T. Y.; Dai, S.; Jaroniec, M.; Qiao, S. Z. *J. Am. Chem. Soc.* **2014**, *136*, 13925.
(34) Gao, M. R.; Sheng, W. C.; Zhuang, Z. B.; Fang, Q. R.; Gu, S.; Jiang, J.; Yan, Y. S. *J. Am. Chem. Soc.* **2014**, *136*, 7077.
(35) Wang, J.; Zhong, H. X.; Qin, Y. L.; Zhang, X. B. *Angew. Chem., Int. Ed.* **2013**, *52*, 5248.
(36) Gong, M.; Zhou, W.; Tsai, M. C.; Zhou, J. G.; Guan, M. Y.; Lin, M. C.; Zhang, B.; Hu, Y. F.; Wang, D. Y.; Yang, J.; Pennycook, S. J.; Hwang, B. J.; Dai, H. J. *Nat. Commun.* **2014**, *5*, 4695.
(37) Song, F.; Hu, X. L. *J. Am. Chem. Soc.* **2014**, *136*, 16481.
(38) Li, Y. G.; Hasin, P.; Wu, Y. Y. *Adv. Mater.* **2010**, *22*, 1926.
(39) McCrory, C. C. L.; Jung, S. H.; Peters, J. C.; Jaramillo, T. F. *J. Am. Chem. Soc.* **2013**, *135*, 16977.
(40) Sun, Y. F.; Gao, S.; Lei, F. C.; Liu, J. W.; Liang, L.; Xie, Y. *Chem. Sci.* **2014**, *5*, 3976.
(41) Zhang, G. Q.; Lou, X. W. *Adv. Mater.* **2013**, *25*, 976.
(42) Lv, X.; Zhu, Y.; Jiang, H.; Yang, X.; Liu, Y.; Su, Y.; Huang, J.; Yao, Y.; Li, C. *Dalton Trans.* **2015**, *44*, 4148.

DOI: 10.1021/jacs.5b02465
J. Am. Chem. Soc. 2015, 137, 5590−5595